AIAA JOURNAL
Vol. 33, No. 10, October 1995

Axisymmetric Oscillations of an Opposing Jet from a Hemispherical Nose

Masahiro Fujita*
Tokyo University, Tokyo 113, Japan

The flowfield around a hemispherical nose with a sonic opposing jet in a freestream of Mach 2.5 is computed by a time-accurate algorithm using the axisymmetric Navier–Stokes equations. Five total pressure ratios of a jet to a freestream, 0.816 ∼ 1.633, are examined. The results obtained strongly depend on the total pressure ratio as the previous experimental results did. In some cases, the computed flowfield oscillates intensely in which the drastic change of the jet structure and the surrounding pressure takes place. The flowfield changes from the stable flow to the unstable flow for the same total pressure ratio as in the experiment. The mechanism of the oscillations and the condition of transition between both types of flow are interpreted physically on the basis of unsteady numerical solutions here.

Nomenclature

c = sound speed
d = jet exit diameter
e = total energy per unit volume
J = transformation Jacobian
Pr = Prandtl number for air
p = pressure
Re = Reynolds number based on the body diameter and the freestream condition
r = spatial coordinate normal to the body axis
t = nondimensional time based on the body diameter and the freestream sound speed
U = contravariant velocity component along the ξ axis
u = velocity component along the x axis
V = contravariant velocity component along the η axis
v = velocity component along the r axis
x = spatial coordinate along the body axis
γ = specific heat ratio
η = transformed coordinate normal to the body
μ = viscosity coefficient
ξ = transformed coordinate along the body
ρ = density
ϕ = angle from stagnation point along the body surface

Subscripts

j = values of the opposing jet
∞ = evaluated in the freestream
0 = stagnation values

Superscripts

n = evaluated at time $n\Delta t$
$'$ = evaluated behind the bow shock

Introduction

THE opposing jet problem has attracted many researchers for a long time not only because of the good applications but also of the physical complexity.[1,2] The oscillation of the flowfield observed in some conditions of the jet has been one of the most interesting problems. It has been clarified in previous studies that the primary parameter that affects the flowfield is the ratio of a jet total pressure to a freestream total pressure.[3–5] When the total pressure ratio is more than a critical value, the flowfield is almost stable, and a Mach disk can be clearly observed inside the jet (denoted as stable flow). When the total pressure ratio is under this value, the flowfield becomes unstable, and the bow shock oscillates intensely (denoted as unstable flow). The critical value of the total pressure ratio depends on a freestream Mach number and a jet exit Mach number. Near the critical value, the flowfield results in either stable or unstable flow, and it tends to alter from one to another in turn (denoted as transition).

Previous studies were mainly intended to clarify the structure of the stable flow and made no detailed analysis of the unstable flow and the transition.[6–8] It is mainly due to the difficulties in the measurement of time variation of flow characteristics, such as bow shock or pressure on the body surface, in the wind tunnel tests. The present study attempts to give a reasonable interpretation of the mechanism of the oscillations by a method of a computation. It is emphasized that the present computation intends not to simulate the real flowfield but to solve the simplified equations of fluid on condition that they preserve essential properties of the flow to obtain the primary phenomenon in the problem.

In this study, the opposing jet problem is discussed on the basis of the previous freejet studies, and the existing wind tunnel test on the opposing jet flow is refereed directly.

Numerical Method

Governing Equations

It has been indicated in the previous experiments that the actual oscillating flowfields are not always axially symmetrical in spite of the employment of an axisymmetric model without an angle of attack. In the present study, however, an axisymmetric flow model is applied on the hypothesis that the essential mechanism of oscillations can be explained by the axisymmetric flow theory. This approach also allows us to save computational time. The derivation of the axisymmetric form from the original three-dimensional equations has been described in the Appendix of the original paper.[9]

In the flowfield discussed here, the Reynolds number is high enough that the returning jet and recirculating flow can be considered to be fully turbulent. But the frequency of the oscillations discussed here is much lower than that of usual turbulent fluctuations of freejets,[10–12] and it has been showed by previous investigations of the freejet that the jet boundary in the vicinity of the jet exit remains laminar.[13] Thus it is assumed that the turbulence effect does not directly affect the oscillations of the flowfield. Under the preceding assumptions, no turbulent model will be used here.

In the present computation, the subgrid for the jet nozzle is included to give the emanating jet condition more accurately. That is, the jet condition has been directly imposed on the jet inlet in the

---

Presented as Paper 94-0659 at the AIAA 32nd Aerospace Sciences Meeting, Reno, NV, Jan. 10–13, 1994; received Feb. 7, 1994; revision received March 13, 1995; accepted for publication March 15, 1995.

*Research Fellow, Japan Society for the Promotion of Science, Department of Aeronautics and Astronautics, 7-3-1, Hongo, Bunkyo; currently Senior Research Associate, Simulation Technology Department, Mitsubishi Research Institute, Inc., 2-3-6, Otemachi, Chiyoda, Tokyo 100, Japan. Member AIAA.

subgrid as the jet chamber condition, because the jet flow there is almost still. Consequently, the jet exit flow at the nozzle throat that contains the boundary layer at the nozzle wall and the curved sonic line could be computed precisely without imposing the uniform flow as the specified boundary condition. The subgrid can be easily included by use of the fortified solution algorithm (FSA) described later. The additional load for the subgrid based on the number of the present grid points is less than 7% of all computational load per iteration.

The governing equations are solved on each grid by turns. Then the FSA,[14,15] in which the forcing terms are added to the governing equations, is applied to connect the subgrid with the main grid. The modified nondimensionalized axisymmetric Navier–Stokes equations transformed to general curvilinear coordinates are

$$\frac{\partial \hat{\boldsymbol{Q}}}{\partial t}+\frac{\partial \hat{\boldsymbol{F}}}{\partial \xi}+\frac{\partial \hat{\boldsymbol{G}}}{\partial \eta}+\hat{\boldsymbol{H}}=\frac{1}{Re}\left(\frac{\partial \hat{\boldsymbol{F}}_v}{\partial \xi}+\frac{\partial \hat{\boldsymbol{G}}_v}{\partial \eta}+\hat{\boldsymbol{H}}_v\right)$$
$$+3\chi(\hat{\boldsymbol{Q}}_f-\hat{\boldsymbol{Q}}) \tag{1}$$

where the switching parameter χ is set to be sufficiently large compared with all of the other terms in the interface region of both grids. In other region, χ is set to be zero. Then $\hat{\boldsymbol{Q}}_f$ represents the fortified solution, which indicates the solution on the another grid. That is, when the equations are solved on the main grid, values in the interface region are set to be the solution obtained on the subgrid just before, whereas when the equations are solved on the subgrid, values in the interface region are set to be the solution obtained on the main grid just before. The high accuracy of the algorithm is maintained in the interface region as well, because the grid points there exactly coincide with each other, and no interpolation is used to transfer solutions between both grids. The basic concept of the FSA is described in the Appendix.

Each vector in both members of the equations is expressed as

$$\hat{\boldsymbol{Q}}=\frac{1}{J}\begin{bmatrix}\rho\\ \rho u\\ \rho v\\ e\end{bmatrix} \qquad \hat{\boldsymbol{F}}=\frac{1}{J}\begin{bmatrix}\rho U\\ \rho uU+\xi_x p\\ \rho vU+\xi_r p\\ (e+p)U\end{bmatrix}$$

$$\hat{\boldsymbol{G}}=\frac{1}{J}\begin{bmatrix}\rho V\\ \rho uV+\eta_x p\\ \rho vV+\eta_r p\\ (e+p)V\end{bmatrix} \qquad \hat{\boldsymbol{H}}=\frac{1}{J}\begin{bmatrix}\rho v/r\\ \rho uv/r\\ \rho v^2/r\\ (e+p)v/r\end{bmatrix}$$

$$\hat{\boldsymbol{F}}_v=\frac{1}{J}\begin{bmatrix}0\\ \xi_x\tau_{xx}+\xi_r\tau_{xr}\\ \xi_x\tau_{xr}+\xi_r\tau_{rr}\\ \xi_x\beta_x+\xi_r\beta_r\end{bmatrix} \qquad \hat{\boldsymbol{G}}_v=\frac{1}{J}\begin{bmatrix}0\\ \eta_x\tau_{xx}+\eta_r\tau_{xr}\\ \eta_x\tau_{xr}+\eta_r\tau_{rr}\\ \eta_x\beta_x+\eta_r\beta_r\end{bmatrix}$$

$$\hat{\boldsymbol{H}}_v=\frac{1}{J}\begin{bmatrix}0\\ \tau_{xr}/r\\ \sigma/r\\ \beta_r/r\end{bmatrix} \tag{2}$$

The stress and heat flux terms in the viscous fluxes are expressed as

$$\begin{aligned}\tau_{xx}&=\frac{1}{3}\mu\left[4(\xi_x u_\xi+\eta_x u_\eta)-2(\xi_r v_\xi+\eta_r v_\eta)-\frac{2v}{r}\right]\\ \tau_{rr}&=\frac{1}{3}\mu\left[4(\xi_r v_\xi+\eta_r v_\eta)-2(\xi_x u_\xi+\eta_x u_\eta)-\frac{2v}{r}\right]\\ \tau_{xr}&=\mu(\xi_r u_\xi+\eta_r u_\eta+\xi_x v_\xi+\eta_x v_\eta)\\ \sigma&=2\mu\left(\xi_r v_\xi+\eta_r v_\eta-\frac{v}{r}\right)\\ \beta_x&=u\tau_{xx}+v\tau_{xr}+\frac{\mu}{Pr(\gamma-1)}\left(\xi_x c_\xi^2+\eta_x c_\eta^2\right)\\ \beta_r&=u\tau_{xr}+v\tau_{rr}+\frac{\mu}{Pr(\gamma-1)}\left(\xi_r c_\xi^2+\eta_r c_\eta^2\right)\end{aligned} \tag{3}$$

For the present flow condition, the air is assumed to have constant specific heat and obey the state equation of a perfect gas. Note that the ratio of specific heat γ is set to be 1.4, the Prandtl number Pr is assumed to be 0.72, and the viscosity coefficient μ is obtained through Sutherland's formula.

Solution Algorithm

These equations are solved by the finite difference method, and unsteady solutions are obtained at each time step through a time-marching procedure. The Lax–Wendroff type explicit total variation diminishing (TVD) scheme, proposed by Yee,[16] is used to solve the discretized equations. The author has applied this scheme to several problems[17,18] to date and obtained satisfactory results in each case. The scheme is temporally and spatially second-order accurate and is suitable for the unsteady problem like the one in this paper as well as steady ones.

The original scheme developed by Yee is applied to one-dimensional systems, and it is necessary to extend it to the multidimensional scheme to apply to the axisymmetric Navier–Stokes equations. Preserving the original second-order time accuracy, the extension can be accomplished by, for example, a Strang type fractional step method.[19] Using this method, the governing equations are at first decomposed into three equations as

$$\frac{\partial \hat{\boldsymbol{Q}}}{\partial t}+\frac{\partial \hat{\boldsymbol{F}}}{\partial \xi}=\frac{1}{Re}\cdot\frac{\partial \hat{\boldsymbol{F}}_v}{\partial \xi}+\chi(\hat{\boldsymbol{Q}}_f-\hat{\boldsymbol{Q}}) \tag{4a}$$

$$\frac{\partial \hat{\boldsymbol{Q}}}{\partial t}+\frac{\partial \hat{\boldsymbol{G}}}{\partial \eta}=\frac{1}{Re}\cdot\frac{\partial \hat{\boldsymbol{G}}_v}{\partial \eta}+\chi(\hat{\boldsymbol{Q}}_f-\hat{\boldsymbol{Q}}) \tag{4b}$$

$$\frac{\partial \hat{\boldsymbol{Q}}}{\partial t}+\hat{\boldsymbol{H}}=\frac{1}{Re}\hat{\boldsymbol{H}}_v+\chi(\hat{\boldsymbol{Q}}_f-\hat{\boldsymbol{Q}}) \tag{4c}$$

Then the solution at the next time step is obtained as

$$\hat{\boldsymbol{Q}}^{n+1}=\mathcal{L}_\xi^{h/2}\mathcal{L}_\eta^{h/2}\mathcal{L}_s^{h}\mathcal{L}_\eta^{h/2}\mathcal{L}_\xi^{h/2}\hat{\boldsymbol{Q}}^n \tag{5}$$

where operators $\mathcal{L}_\xi^h$, $\mathcal{L}_\eta^h$, and $\mathcal{L}_s^h$ are implemented for Eqs. (4a–4c) with $h=\Delta t$, respectively. Both operators $\mathcal{L}_\xi^h$ and $\mathcal{L}_\eta^h$ represent the second-order Lax–Wendroff explicit TVD differencing for convective terms and second-order central differencing for diffusive terms. In the case of ξ direction, the solution algorithm is expressed so that the forcing term is treated properly in the solution process as

$$\mathcal{L}_\xi^h\!: \quad \begin{aligned}\hat{\boldsymbol{Q}}^{n+1}&=\hat{\boldsymbol{Q}}^n-\frac{h}{1+h\chi}\left(\partial_\xi\hat{\boldsymbol{F}}-\frac{1}{Re}\partial_\xi\hat{\boldsymbol{F}}_v\right)^n\\ &\quad+\frac{h\chi}{1+h\chi}(\hat{\boldsymbol{Q}}_f-\hat{\boldsymbol{Q}}^n)\end{aligned} \tag{6}$$

The algorithm can be expressed in the same manner in the η direction. The operator $\mathcal{L}_s^h$, on the other hand, denotes a second-order Runge–Kutta method for both convective and diffusive source terms as follows:

$$\hat{\boldsymbol{Q}}^*=\hat{\boldsymbol{Q}}^n-\frac{h}{1+h\chi}\left(\hat{\boldsymbol{H}}-\frac{1}{Re}\hat{\boldsymbol{H}}_v\right)^n+\frac{h\chi}{1+h\chi}(\hat{\boldsymbol{Q}}_f-\hat{\boldsymbol{Q}}^n) \tag{7a}$$

$\mathcal{L}_s^h$:

$$\hat{\boldsymbol{Q}}^{n+1}=\frac{1}{2}\left[\hat{\boldsymbol{Q}}^n+\frac{h\chi}{1+h\chi}(\hat{\boldsymbol{Q}}_f-\hat{\boldsymbol{Q}}^n)\right]+\frac{1}{2}\left[\hat{\boldsymbol{Q}}^*-\frac{h}{1+h\chi}\left(\hat{\boldsymbol{H}}-\frac{1}{Re}\hat{\boldsymbol{H}}_v\right)^*\right] \tag{7b}$$

In each case, it is obvious on inspection that the algorithm reduces to the standard one for $\chi=0$ and it gives simply $\hat{\boldsymbol{Q}}^{n+1}=\hat{\boldsymbol{Q}}_f$ for $\chi\gg 1$.

Grid System and Boundary Conditions

The configuration of the model employed in the wind tunnel experiment[20] is also used in the present study. The jet exit is placed on the stagnation point of the hemispherical nose, and its diameter is equal to one-tenth of the body diameter. The domain of interest is limited to the region that is bounded by the bow shock and the body. Thus the main grid including 180 × 130 points is placed on the body-fitting curvilinear coordinates, and the subgrid including 43 × 40 points is inserted into the sonic jet nozzle. The present grid system is shown in Fig. 1. The grid points are clustered in the vicinity of the body surface, the nozzle wall, and the jet exit region. All solutions to be described later, including the case without a jet, have been obtained using the same computational grid here. The flowfield was computed using coarser grids as a preliminary study. It was found from the result that using a fine grid gives the same solutions of unsteady flow as coarser grids, except slightly high resolution of shocks and shear layers. Thus it can be concluded that the present numerical solutions have converged to the mathematical solutions.

The boundary conditions on each boundary of the computational domain are implemented numerically as follows. On the main grid, the variables on the inflow boundary are fixed to freestream values. On the outflow boundary, the variables are given by linear extrapolation from variables on the internal grid points. Those on the body surface are given by no-slip, zero-pressure-gradient, and adiabatic wall conditions. On the symmetric axis, zero-order extrapolation is practical since this represents absence of flux condition across the axis. On the other hand, in case of the subgrid, the same boundary conditions as the main grid are implemented on the nozzle wall and the symmetrical axis. At the nozzle inlet, the density and the pressure are specified according to the prescribed total pressure ratio and the total temperature. The velocities there are given by the zero-order extrapolation from the downstream points under parallel flow condition. Finally, the values on the jet exit boundary on each grid are fortified in turn to the solution on the another grid.

The initial condition corresponds to an impulsive start. Before start of calculations, the values on all inner grid points of the main grid are initialized to those of a freestream, and those of the subgrid are given as the analytical quasi-one-dimensional solution in the sonic nozzle.

Flow Conditions

As described before, the existing experimental data[20] are used as the basis for the present study. The time-averaged pressure on the body surface and normal schlieren photographs are available for the comparisons between the experiment and the present computation. Since the objective of this study is to clarify the cause of a physical phenomenon, the present computation has been carried out on one case of the experimental results, in which the freestream Mach number and the jet exit Mach number are 2.5 and 1.0, respectively. The flow parameters are shown in Table 1.

Table 1 Flow conditions

Freestream	Re	1.47×10^6
	M_∞	2.5
	$T_{0\infty}$, K	294
Opposing jet	M_j	1.0
	T_{0j}, K	294
	$P_{0j}/P_{0\infty}$	0.816~1.633

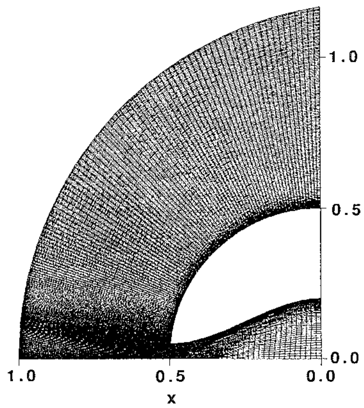

Fig. 1 Computational grid system.

Results and Discussions

Comparisons with Experiment

Five total pressure ratios of a jet to a freestream are examined to obtain the stable, unstable, and transitional flow. Figure 2 shows the variation of the time-averaged body surface pressure at 15-deg position measured from the symmetric axis. This position is located in the recirculating region in every cases discussed here. An abrupt rise of the pressure at a certain total pressure ratio corresponds to the transition from an unstable flow to a stable flow. The computed and experimental pressure curves agree qualitatively. The transition occurs at nearly the same total pressure ratio both in the computation and in the experiment.

A series of numerical solutions obtained at each time step are averaged in time for comparison with the experiment. The upper half of Fig. 3a illustrates the time-averaged density contours for the stable flow. Comparing with the schlieren photograph shown in the lower half, it can be said that the shapes and locations of the bow shock and the Mach disk agree well with each other. In the upper half

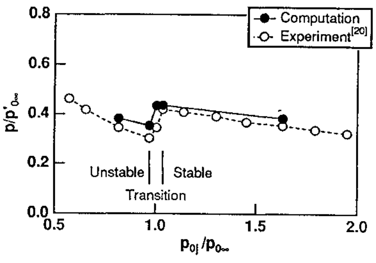

Fig. 2 Surface pressure in recirculating region vs total pressure ratio.

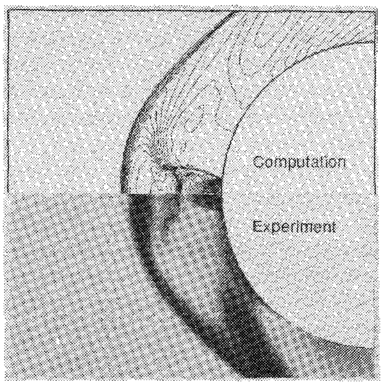

a) Stable flow ($p_{0j}/p_{0\infty} = 1.633$)

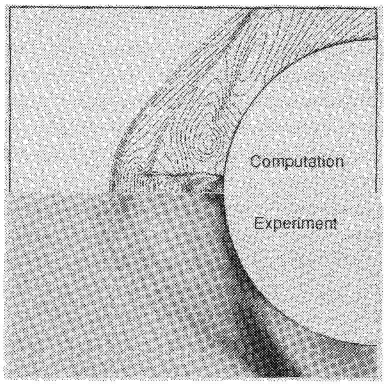

b) Unstable flow ($p_{0j}/p_{0\infty} = 0.816$)

Fig. 3 Time-averaged density contours and schlieren photographs.

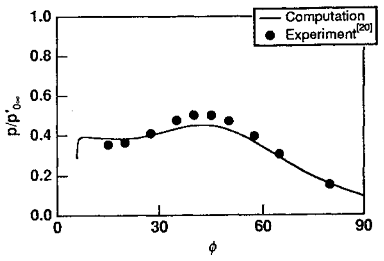

a) Stable flow ($p_{0j}/p_{0\infty} = 1.633$)

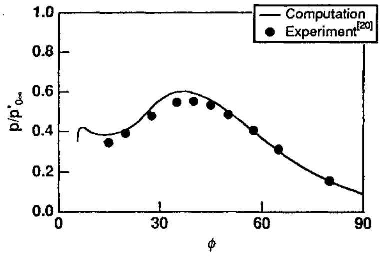

b) Unstable flow ($p_{0j}/p_{0\infty} = 0.816$)

Fig. 4 Time-averaged surface pressure distribution.

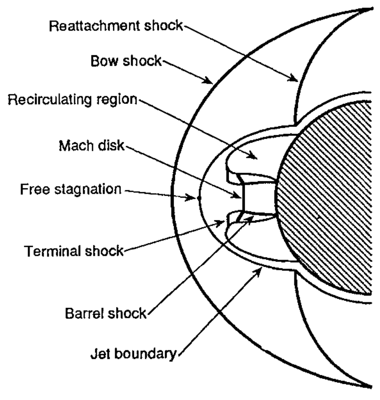

Fig. 5 Stable flow model.

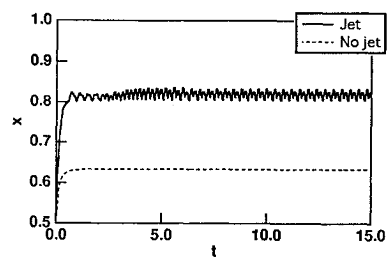

a) Stable flow ($p_{0j}/p_{0\infty} = 1.633$)

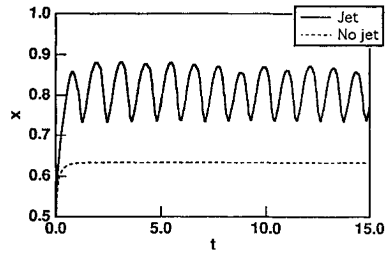

b) Unstable flow ($p_{0j}/p_{0\infty} = 0.816$)

Fig. 6 Time history of bow shock on axis.

of Fig. 3b, the time-averaged density contours for the unstable flow are illustrated. Contrary to the stable flow case, contours of the bow shock and the Mach disk are obscured, which seems to agree with the schlieren photograph shown in the lower half. This may suggest that the bow shock and Mach disk oscillate at a considerably large amplitude, and the period of oscillation is much shorter than the exposure time.

Comparisons of the surface pressure distribution between the time-averaged numerical solutions and the experimental data are shown in Figs. 4a and 4b. Considerable decrease in pressure around the jet occurs as a result of a large separation of the jet flow. In both figures, pressure curves obtained from the computation agree fairly well with the experimental data.

As a result of these comparisons, it was shown that many features of the opposing jet flow observed in the experiments, such as the existence of stable and unstable flow and the transition between them, can be explained through the numerical solution. Therefore, the accuracy of the simplified flow model used under the assumption of the axisymmetric flow can be considered as satisfactory in resolving the opposing jet flowfield.

Stable Flow

Some researchers have already developed models of explaining stable flow.[6,8] A more precise model of explaining stable flow is suggested here, on basis of the time-averaged numerical solutions described earlier. Figure 5 shows a new flow model developed in the present study. Although this model is roughly similar to previous ones, special attention is paid to the structure of the jet. It is illustrated that the supersonic flow, which passes the barrel shock and the reflected shock emanating the triple point, is finally decelerated to subsonic speed by a terminal shock. There is a subsonic pocket around the symmetrical axis bounded by the bow shock, the Mach disk, and the terminal shock. The fluid, which is nearly still in the subsonic pocket, begins to flow downstream along the jet boundary and is accelerated again to supersonic speed.

The existence of a slight unsteadiness has also been reported even for the stable flow case.[6] Figure 6a shows the time history of the bow shock on the symmetrical axis for the stable flow, where the entire flowfield is expected to be nearly stable. The solution oscillates about its neutral position in an amplitude less than the width of the thick line representing a bow shock in the photograph. An oscillation with an amplitude this small cannot be found in a normal schlieren photograph. Thus, this oscillatory solution may correspond to the small oscillation described in previous studies.

Unstable Flow

Time Variation of Flowfield

Figure 6b shows the time histories of the bow shock on the symmetrical axis for the unstable flow. Contrary to the stable flow case, the computed flowfield exhibits a nearly periodic oscillation with large amplitude. The distance between the stagnation point and the bow shock, measured along the symmetrical axis, reaches up to 2.8 times as that of the no-jet case, and its amplitude is about 15% of the body diameter. Although there are no quantitative experimental data to confirm this solution, it appears that this represents the oscillatory flow observed in the wind tunnel experiments.

For the unstable flow case, the drastic change of the jet structure is illustrated in a time series of instantaneous flowfields. Figures 7a–7h show changes of the flowfield during the period of oscillation by density contours. The solution on the subgrid is not shown here, because there is no change of the flowfield in the nozzle after a steady oscillatory solution in the main grid has been reached. The sequence of the figures starts from the stage when the jet length is shortest in the period of oscillation, as shown in Fig. 7a. At this moment, the supersonic jet terminates through a nearly normal shock (Mach disk) and immediately loses its total pressure down to the value of the free stagnation. The structure of the first cell of the jet changes with time to the regular reflection type, and the second cell of the jet appears following the first cell as shown in Figs. 7b and 7c. As a result, the jet length gradually increases so that both the bow shock and the free stagnation also move away from the body, although the position of the free stagnation is not discernible in the figures. At this phase, the jet flow experiences a pair of oblique shocks in the first cell, until being terminated by a normal shock in the second cell, after which a longer distance is required to lose its total pressure completely down to the value of the free stagnation.

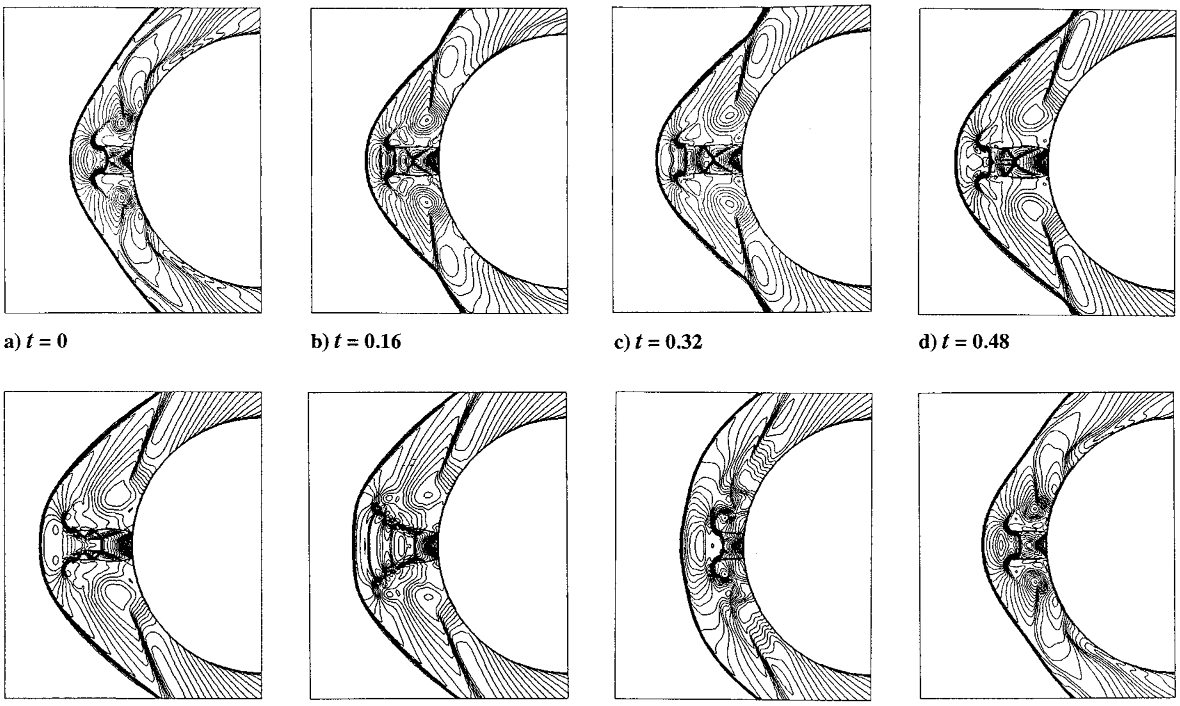

a) $t = 0$ b) $t = 0.16$ c) $t = 0.32$ d) $t = 0.48$

e) $t = 0.64$ f) $t = 0.80$ g) $t = 0.96$ h) $t = 1.12$

Fig. 7 Time history of unstable flowfield.

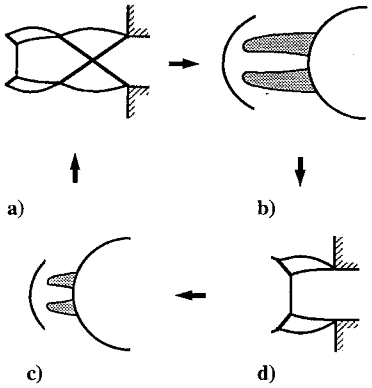

Fig. 8 Oscillatory flow model.

In Fig. 7d, an abrupt transition of the shock structure in the first cell occurs, when the regular reflection of the barrel shocks changes to the Mach reflection. This is followed by the increase in the diameter of the Mach disk, when the entire flow after the Mach disk becomes subsonic, so that the Mach disk at the end of the second cell disappears, as shown in Fig. 7e. The disappearance of the Mach disk in the second cell means the breakdown of the second cell, which is clearly visible in Fig. 7f. Subsequently, the jet length is suddenly shortened, so that the bow shock and the free stagnation also begin to move back toward the body, i.e., to the position as shown in Fig. 7g. Consequently, the length of the first jet cell returns to the original value at the end of the period, and a shape of the jet nearly identical to the original one, as shown in Fig. 7h.

Oscillatory Flow Model

Love et al.[21] made a detailed experimental and theoretical study of axisymmetric freejets. Their most important finding was that the jet structure changes from the Mach reflection type to the regular reflection type, when the surrounding pressure is more than one-half of the jet exit pressure. On the basis of the preceding finding on a freejet, a model of the oscillation for the unstable flow is developed, as illustrated in Fig. 8.

At the beginning of the cycle in Fig. 8a, where the bow shock is at the most backward position in the period of oscillation and the volume of recirculating region is at the minimum, there is only one jet cell, which contains a normal shock at the end. At this time, the pressure in the recirculating region, i.e., the pressure surrounding jet, gives the maximum value, which is more than the threshold value of the change of jet structure, as shown in Fig. 8b. Consequently, the structure of first jet cell rapidly changes to the regular reflection type, which is generally called slightly underexpanded jet, whereby a second cell appears ahead of the first cell, as shown in Fig. 8c. This means that the length of the jet, defined as the distance from the jet exit to the free stagnation, increases with time. The length of the jet is at the maximum value when the free stagnation point reaches its most forward position. In this phase, the long jet including two cells increases the volume of the recirculating region, reducing its pressure. As a result, the pressure surrounding the jet may become less than the threshold value of the change of the jet structure, and the structure of the first cell changes to the Mach reflection type, which is called highly underexpanded jet as shown in Fig. 8d. After this change, the flow passing the Mach disk in the first cell becomes subsonic, which causes the second cell to disappear instantly. The free stagnation now rapidly moves backward, i.e., the length of the jet decreases with time. Finally the length of the jet gives its minimum value again, at which time the volume of the recirculating region is also at its minimum, as shown in Fig. 8a. The change of the flowfield repeats in this cycle.

Transition

Finley[6] has suggested the condition of transition between the stable and unstable flow by a theoretical analysis. According to Finley, the transition occurs at the total pressure ratio at which the location of the jet terminal shock coincides with that of the first intersection of barrel shocks in a jet cell. The location of the jet terminal shock satisfies the static condition of the opposing jet. On the other hand, the location of the first intersection of barrel shocks coincides with that of an equivalent freejet, whose surrounding pressure is equal to the pressure in the recirculating region. The condition of Finley will be validated here quantitatively, on the basis of the present numerical results. To discuss Finley's condition, it is necessary to obtain the location of the Mach disk and the shock intersection on the axis as a function of the total pressure ratio. The distance from jet exit to the Mach disk that is required to attain the static condition has been calculated by Romeo and Sterrett,[22] using the formula of Ashkenas and Sherman,[23] which expresses the total pressure distribution along the centerline of a sonic freejet. Furthermore, Love et al.[21] have measured the location of the first intersection of barrel shocks

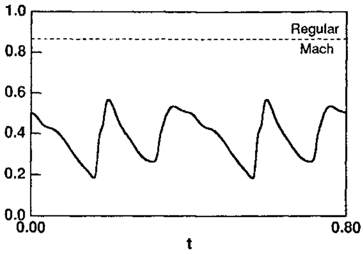

a) Stable flow ($p_{0j}/p_{0\infty}$ = 1.633)

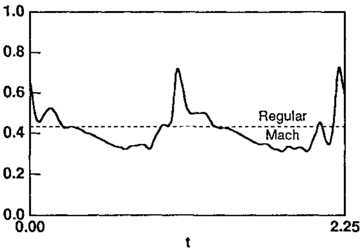

b) Unstable flow ($p_{0j}/p_{0\infty}$ = 0.816)

Fig. 9 Time history of pressure in recirculating region.

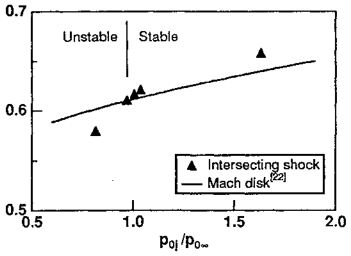

Fig. 10 Location of intersecting shock and Mach disk vs total pressure ratio.

on the axis as a function of a ratio of the jet exit pressure to the surrounding pressure. In the case of opposing jet flow, it is necessary to use the value of computed pressure in the recirculating region as that of the surrounding pressure.

Figure 9 shows the time history of the pressure in the recirculating region. The pressure tends to oscillate considerably with time for both stable and unstable flow cases. In the stable flow case ($p_{0j}/p_{0\infty} = 1.633$) as in Fig. 9a, the amplitude of each oscillation of the surrounding pressure is nearly constant, and no abrupt peak exists. On the other hand, in the unstable flow case ($p_{0j}/p_{0\infty} = 0.816$) as in Fig. 9b, steep peaks of the pressure can be observed that are due to the impingement of the broken jet flow on the body surface. The thresholds of transition of the shock reflection in the first jet cell are also shown in these figures. Each dashed line represents the threshold, under which the Mach reflection exists whereas over which the regular reflection appears. In the stable flow case, the surrounding pressure is under the threshold throughout the period, i.e., only the Mach reflection appears. This corresponds well with the observations of the computed density contours. To the contrary, in the unstable flow case, the surrounding pressure occasionally exceeds the threshold, so that both types of reflection appear in a single period. As is described earlier, the surrounding pressure oscillates intensely in both cases, and thus time-averaged values are employed for the present estimation.

Figure 10 gives the variation of the location of the shock intersection with the total pressure ratio. The curve represents the location of the Mach disk. As shown in this figure, the location of the intersecting shock coincides with that of the Mach disk, when the total pressure ratio is about 1.0. Above this value, the distance from the stagnation point to the intersecting shock is larger than that to Mach disk, so that the incoming flow to the Mach disk is not disturbed by any shock wave. On the other hand, under the value, the barrel shocks intersect with each other on the axis before the Mach disk, so that the expanding flow terminates at the intersecting point. As a result, a second jet cell appears before the terminal Mach disk. If Finley's condition is applied, it is anticipated that the flowfield becomes stable above the total pressure ratio of 1.0. This prediction agrees quite well with the computation here as well as the experimental result. Therefore it is satisfactory to say that Finley's condition is quantitatively validated.

Concluding Remarks

A model that explains the mechanism of oscillations of an opposing jet from a hemispherical nose has been developed in the present study. Based on the analysis of the numerical solutions and the existing experimental results, the following conclusions can be drawn.

1) The computations have successfully reproduced the oscillations in the stable and the unstable flows as well as the transition between both flows. The time-averaged pressure on body surface and the threshold of transition agree quantitatively with the experimental data.

2) In the unstable flow case, the changes of the jet structure and the pressure in the recirculating region function as a feedback mechanism. Thus a self-excited oscillation of the flowfield occurs between two possible equilibrium states.

3) It has been quantitatively validated by the present numerical solutions that Finley's condition represents the condition of transition between stable and unstable flows.

An another case was computed, in which the jet condition was specified simply as the boundary condition at the jet exit. The result showed no significant difference from the present case except slight discrepancies in the periods of oscillation and the surface pressure near the jet exit. However, further consideration should be given to clarify the effect of the nonuniform jet exit flow. The author expects that a new path has opened in the research of oscillatory opposing jet flow by the present study and is also convinced that the validity of the present flow models will be demonstrated by further studies.

Appendix: FSA

The FSA is based on the fortified Navier–Stokes (FNS) approach developed by Van Dalsem and Steger.[24,25] In the original FNS approach, the solution of the boundary-layer equation has been added to the Navier–Stokes equations as a forcing term to improve the efficiency and the accuracy of an algorithm. Based on their work, Fujii has applied the FNS concept to zonal grids that are used for complex configurations. This is called the FSA for generality, because the governing equations do not need to be the Navier–Stokes equations in his approach. In short, the FSA utilizes the FNS concept to transfer the information of the connected zones among each other.

In the FSA as well as the FNS, the forcing term $\chi(\hat{Q}_f - \hat{Q})$, including a switching parameter χ, is added to the governing equations. For $\chi \gg 1$, the forcing term becomes excessively large compared with all of the other terms, so that the equations are reduced to just $\hat{Q} = \hat{Q}_f$, i.e., the $\hat{Q}_f$ variables are fortified. To the contrary, for $\chi = 0$, the forcing term vanishes and the original equations reappear. In this way, one can force any solution $\hat{Q}_f$ at some portion of the computational domain, where a very large χ is given as the switching parameter.

Using the modified equations described earlier, a zonal method is defined. Consider a slightly overlapped zonal grid in which the grid points on zone 1 and zone 2 coincide with each other. When zone 1 is solved, if χ is set to be sufficiently large and $\hat{Q}_f$ variables are specified by $\hat{Q}$ of zone 2 at the previous time step, the solution on zone 2 is automatically fortified in the overlapping boundary region. The same is true for zone 2 when zone 2 is solved. In this way, the solution on the other grid is given as the interface boundary condition of one grid, and the algorithm can maintain high-order accuracy at the grid interface. Detailed features and some applications of the FSA are described in the papers of Fujii et al.[14] and Fujii.[15]

Acknowledgments

This research was supported in part by scientific research funds from the Ministry of Education. Special thanks are due to K. Karashima and K. Sato of the Institute of Space and Astronautical Science for offering the use of their unpublished experimental data.

References

[1] Warren, C. H. E., "An Experimental Investigation of the Effect of Ejecting a Coolant Gas at the Nose of a Bluff Body," *Journal of Fluid Mechanics*, Vol. 8, Pt. 3, 1960, pp. 400–417.

[2] Charczenko, N., and Hennessey, K. W., "Investigation of a Retrorocket Exhausting from the Nose of a Blunt Body into a Supersonic Free Stream," NASA TN D-751, Sept. 1961.

[3] Hayman, L. O., Jr., "Jet Effects on Cylindrical Afterbodies Housing Sonic and Supersonic Nozzles Which Exhaust Against a Supersonic Stream at Angles of Attack from 90 deg to 180 deg," NASA TN D-1016, March 1962.

[4] Romeo, D. J., and Sterret, J. R., "Exploratory Investigation of the Effect of a Forward Facing Jet on the Bow Shock of a Blunt Body in a Mach Number 6 Free Stream," NASA TN D-1605, Feb. 1963.

[5] Karashima, K., and Sato, K., "An Experimental Study of an Opposing Jet," *Bulletin of Institute of Space and Astronautical Science*, Vol. 11, No. 1(A), 1975, pp. 53–64.

[6] Finley, P. J., "The Flow of a Jet from a Body Opposing a Supersonic Free Stream," *Journal of Fluid Mechanics*, Vol. 26, Pt. 2, 1966, pp. 337–368.

[7] Satofuka, N., and Matsuno, N., "Numerical Calculation of the Interaction Between Opposing Jets and Supersonic Free Stream," *Journal of Japan Society for Aeronautical and Space Sciences*, Vol. 23, No. 262, 1975, pp. 586–595.

[8] Fox, J. H., "Counterflow Sonic Nosejet into a Supersonic Stream," AIAA Paper 86-1808, June 1986.

[9] Fujita, M., "Axisymmetric Oscillations of an Opposing Jet from a Hemispherical Nose," Ph.D. Thesis, Dept. of Aeronautics, Univ. of Tokyo, Japan, March 1993.

[10] Powell, A., "On the Mechanism of Choked Jet Noise," *The Physical Society-Section B*, Vol. 66, Pt. 12, 1953, pp. 1039–1056.

[11] Hammitt, A. G., "The Oscillation and Noise of an Overpressure Sonic Jet," *Journal of the Aerospace Sciences*, Vol. 28, No. 9, 1961, pp. 673–680.

[12] Tam, C. K. W., Seiner, J. M., and Yu, J. C., "Proposed Relationship Between Broadband Shock Associated Noise and Screech Tones," *Journal of Sound and Vibration*, Vol. 110, No. 2, 1986, pp. 309–321.

[13] Kawamura, R., "Study on Axially Symmetric Supersonic Jets with Special Regard to the Shock Waves in Them," *Report of Institute of Science and Technology*, Vol. 6, No. 3, 1952, pp. 141–148.

[14] Fujii, K., Tamura, Y., and Kuroda, S., "Unified Zonal Method Based on the Fortified Navier–Stokes Concept," AIAA Paper 91-1558, June 1991.

[15] Fujii, K., "Unified Zonal Method Based on the Fortified Solution Algorithm," Inst. of Space and Astronautical Science, Rept. 648, Kanagawa, Japan, Dec. 1992.

[16] Yee, H. C., "A Class of High-Resolution Explicit and Implicit Shock-Capturing Methods," NASA TM 101088, Feb. 1989.

[17] Fujita, M., and Kubota, H., "Numerical Simulation of Flowfield over a Spiked Blunt-Nose," *Computational Fluid Dynamics Journal*, Vol. 1, No. 2, 1992, pp. 187–195.

[18] Fujita, M., and Kubota, H., "Oscillations of an Opposing Jet from a Hemispherical Nose," *Proceedings of 5th International Symposium on Computational Fluid Dynamics* (Sendai, Japan), Japan Society of Computational Fluid Dynamics, Tokyo, Japan, 1993, pp. 215–220.

[19] Strang, G., "On the Construction and Comparison of Difference Schemes," *SIAM Journal on Numerical Analysis*, Vol. 5, Sept. 1968, pp. 506–517.

[20] Karashima, K., and Sato, K., private communication, Inst. of Space and Astronautical Science, July 1992.

[21] Love, E. S., Grigsby, C. E., Lee, L. P., and Woodling, M. J., "Experimental and Theoretical Studies of Axisymmetric Free Jets," NASA TR R-6, 1959.

[22] Romeo, D. J., and Sterrett, J. R., "Flow Field for Sonic Jet Exhausting Counter to a Hypersonic Mainstream," *AIAA Journal*, Vol. 3, No. 3, 1965, pp. 544–546.

[23] Ashkenas, H., and Sherman, F. S., "The Structure and Utilization of Supersonic Free Jets in Low Density Wind Tunnels," *Rarefied Gas Dynamics*, edited by J. H. de Leeuw, Vol. 2, Academic, New York, 1966, pp. 84–105.

[24] Van Dalsem, W. R., and Steger, J. L., "The Fortified Navier–Stokes Approach," Workshop on Computational Fluid Dynamics, Davis, CA, June 1986.

[25] Van Dalsem, W. R., and Steger, J. L., "Using the Boundary-Layer Equations in Three-Dimensional Viscous Flow Simulation," 58th Meeting of the Fluid Dynamics Panel Symposium on Applications of Computational Fluid Dynamics in Aeronautics, No. 24, Aix-en-Provence, France, April 1986.